

## Variable Stars in the Globular Cluster NGC 288: [Fe/H] and Distance\*

A. Arellano Ferro<sup>1,2</sup>, D.M. Bramich<sup>2,3</sup>, S. Giridhar<sup>4</sup>,  
R. Figueroa Jaimes<sup>2,5</sup>, N. Kains<sup>2</sup> and K. Kuppuswamy<sup>4</sup>

<sup>1</sup> Instituto de Astronomía, Universidad Nacional Autónoma de México  
e-mail: armando@astro.unam.mx

<sup>2</sup> European Southern Observatory, Karl-Schwarzschild-Straße 2,  
85748 Garching bei München, Germany

<sup>3</sup> Qatar Environment and Energy Research Institute, Qatar Foundation, Tornado Tower,  
Floor 19, P.O. Box 5825, Doha, Qatar

<sup>4</sup> Indian Institute of Astrophysics, Koramangala 560034, Bangalore, India

<sup>5</sup> SUPA, School of Physics and Astronomy, University of St Andrews, North Haugh,  
St Andrews, KY16 9SS, United Kingdom

*Received November 19, 2013*

### ABSTRACT

A search for variable stars in the globular cluster NGC 288 was carried out using a time-series of CCD images in the  $V$  and  $I$  filters. The photometry of all stellar sources in the field of view of our images, down to  $V \approx 19$  mag, was performed using difference image analysis (DIA). For stars of  $\approx 15$  mag, measurement accuracies of  $\approx 8$  mmag and  $\approx 10$  mmag were achieved for  $V$  and  $I$  respectively. Three independent search strategies were applied to the 5525 light curves but no new variables were found above the threshold limits characteristic of our data set. The use of older data from the literature combined with the present data allowed the refinement of the periods of all known variables. Fourier light curve decomposition was performed for the RRab and the RRc stars to obtain an estimate of  $[\text{Fe}/\text{H}]_{\text{ZW}} = -1.62 \pm 0.02$  (statistical)  $\pm 0.14$  (systematic). A true distance modulus of  $14.768 \pm 0.003$  mag (statistical)  $\pm 0.042$  mag (systematic), or a distance of  $8.99 \pm 0.01$  kpc (statistical)  $\pm 0.17$  kpc (systematic) was calculated from the RRab star. The RRc star predicts a discrepant distance about one kiloparsec shorter but it is possibly a Blazhko variable. An independent distance from the P–L relationship for SX Phe stars leads to a distance of  $8.9 \pm 0.3$  kpc. The SX Phe stars V5 and V9 are found to be double mode pulsators.

**Key words:** *globular clusters: individual: NGC 288 – Stars: variables: RR Lyrae, Stars: variables: delta Scuti*

### 1. Introduction

The globular cluster NGC 288 (C0050-268 in the IAU nomenclature) ( $\alpha = 00^{\text{h}}52^{\text{m}}45^{\text{s}}.2$ ,  $\delta = -26^{\circ}34'57''.4$ , J2000;  $l = 151^{\circ}29$ ,  $b = -89^{\circ}38$ ) lies toward the

\* Based on observations collected with the 2.0 m telescope at the Indian Astrophysical Observatory, Hanle, India.

southern Galactic pole at about 12 kpc from the Galactic center, hence it is subject to very little interstellar reddening,  $E(B - V) = 0.03$  mag (Harris 1996, 2010 update).

The cluster has been studied photometrically since 1943, which has led to the discovery of several variable stars. Using 144 photographic plates from the Franklin-Adams camera at Johannesburg, Oosterhoff (1943) reported the discovery of a long-period ( $\approx 100$  d) semi-regular variable star V1 as the first variable star in NGC 288. The next variable star V2, an RRab star, was discovered about thirty-five years later by Hollingsworth and Liller (1977) using seventeen  $B$  photographic plates and they estimated a period of  $\approx 0.679$  d. It was not until the era of CCD cameras that NGC 288 was studied again for variable stars in a pair of papers by Janusz Kaluzny and collaborators (Kaluzny 1996, Kaluzny, Krzeminski and Nalezyty 1997). These investigators used PSF-fitting photometry to find a new RR Lyr star V3 pulsating in the first-overtone, six SX Phe pulsators (V4–V9), and one eclipsing binary of the W UMa type (V10). Although Pietrukowicz *et al.* (2008) used difference image analysis photometry to search (unsuccessfully) for dwarf novae in time-series CCD images of NGC 288, they did not analyse their data for the known variables or attempt to find any new variables.

Our study to search for variable stars in NGC 288 and our analysis of their characteristics is therefore the first such study using CCD image data and DIA combined.

The distribution of these ten variables in the cluster is rather peculiar as they define an off-center concentration of less than 3 arcmin in diameter in the otherwise  $10 \times 10$  arcmin<sup>2</sup> field of our images. While this distribution may not be very improbable, as will be discussed later in the paper, it added to our interest in exploring the possibility of an incomplete census of variables stars. In the recent past our team has exploited the powerful technique of DIA for time-series CCD images in globular clusters to update and characterise the population of variables in them (*e.g.*, Arellano Ferro *et al.* 2013, 2011, Kains *et al.* 2013, 2012, Figuera Jaimes *et al.* 2013, Bramich *et al.* 2011).

In the present paper we report the results of our variable star search in the  $V$  and  $I$  filters and the calculation of the cluster metallicity and distance. In Section 2 we describe the observations and data reductions. In Section 3 we describe the approaches used to identify new variables and the procedure to refine the periods. In Section 4 we apply Fourier light curve decomposition to the RR Lyr stars V2 and V3 and calculate their metallicity and absolute magnitude, and hence the distance to the cluster. In Section 5 we discuss the SX Phe P–L (Period-Luminosity) relation and use the SX Phe stars as independent indicators of the cluster distance. The double mode nature of V5 and V9 is also discussed there. In Section 6 the properties of the variables V1 and V10 are addressed. In Section 7 we summarise our results.

## 2. Observations and Reductions

The observations employed in the present work were performed using the Johnson–Kron–Cousins  $V$  and  $I$  filters on nine nights during 2010–2013 at the 2.0 m telescope of the Indian Astronomical Observatory (IAO), Hanle, India, located at 4500 m above sea level. The detector was a Thompson CCD of  $2048 \times 2048$  pixels with a pixel scale of 0.296 arcsec/pix translating to a field of view (FoV) of  $\approx 10.1 \times 10.1$  arcmin<sup>2</sup>.

The log of observations is shown in Table 1 in which the dates, number of frames, exposure times and average nightly seeing are recorded. A total of 174 epochs in the  $V$  filter and 201 in the  $I$  filter spanning almost three years were obtained.

Table 1

The distribution of observations of NGC 288 for each filter

Date [y.m.d]	$N_V$	$t_V$ [s]	$N_I$	$t_I$ [s]	Avg seeing ["]
2010.12.11	21	30–80	36	20–25	1.8
2010.12.12	8	80	15	20–60	1.7
2011.10.07	20	80–100	19	15–20	2.5
2011.11.02	23	80–100	24	15–20	2.7
2011.11.03	33	80–150	33	20–30	2.5
2011.11.05	42	80	42	20	2.5
2013.01.20	2	160	2	30	2.7
2013.08.26	18	35–45	20	10–25	1.7
2013.08.27	7	70–90	10	10–20	1.9
Total:	174		201		

Columns  $N_V$  and  $N_I$  represent the number of images taken with the  $V$  and  $I$  filters respectively. Exposure time, or range of exposure times, employed during each night for each filter are listed in the columns  $t_V$  and  $t_I$  and the average seeing in the last column.

### 2.1. Difference Image Analysis

We employed the technique of difference image analysis (DIA) to extract high-precision photometry for all of the point sources in the images of NGC 288 and we used the DANDIA<sup>†</sup> pipeline for the data reduction process (Bramich *et al.* 2013) which includes an algorithm that models the convolution kernel matching the PSF of a pair of images of the same field as a discrete pixel array (Bramich 2008).

In general, a reference image is built by stacking a set of images with the best seeing. However, in the present case the seeing was not particularly good and we

<sup>†</sup>DANDIA is built from the DANIDL library of IDL routines available at <http://www.danidl.co.uk>

opted for using only one image as a reference image for each filter. Then a sequence of difference images was created by subtracting the relevant reference image, convolved with an appropriate spatially variable kernel, from each registered image. The spatially variable convolution kernel for each registered image was determined using bilinear interpolation of a set of kernels that were derived for a uniform  $6 \times 6$  grid of subregions across the image.

The differential fluxes for each star detected in the reference image were measured on each difference image. Light curves for each star were constructed by calculating the total flux  $f_{\text{tot}}(t)$  in ADU/s at each epoch  $t$  from:

$$f_{\text{tot}}(t) = f_{\text{ref}} + \frac{f_{\text{diff}}(t)}{p(t)} \quad (1)$$

where  $f_{\text{ref}}$  is the reference flux [ADU/s],  $f_{\text{diff}}(t)$  is the differential flux [ADU/s] and  $p(t)$  is the photometric scale factor (the integral of the kernel solution). Conversion to instrumental magnitudes was achieved using:

$$m_{\text{ins}}(t) = 25.0 - 2.5 \log [f_{\text{tot}}(t)] \quad (2)$$

where  $m_{\text{ins}}(t)$  is the instrumental magnitude of the star at time  $t$ . Uncertainties were propagated in the correct analytical fashion.

The above procedure and its caveats have been described in detail in Bramich *et al.* (2011).

We also performed a relative self-calibration of the ensemble photometry. We applied the methodology developed in Bramich and Freudling (2012) to solve for the magnitude offsets  $Z_k$  that should be applied to each photometric measurement from the image  $k$ . In terms of DIA, this translates into a correction (to first order) for the systematic error introduced into the photometry from an image due to an error in the fitted value of the photometric scale factor  $p$ . We found that in either filter the magnitude offsets that we derive are of the order of  $\approx 1-10$  mmag with a handful of worse cases reaching  $\approx 30$  mmag. Applying these magnitude offsets to our DIA photometry notably improves the light-curve quality, especially for the brighter stars.

## 2.2. Transformation to the Standard System

Standard stars in the field of NGC 288 are very numerous in the online collection of Stetson (2000)<sup>‡</sup>. We selected a group of standards in the FoV of our images that cover the  $V$  and  $V - I$  ranges between 14.5 mag and 20.5 mag and 0 mag and 1.5 mag, respectively, to ensure a good transformation for most of the full Color–Magnitude Diagram (CMD), and to check for the color dependence of the transformations.

---

<sup>‡</sup><http://www3.cadc-ccda.hia-ihp.nrc-cnrc.gc.ca/community/STETSON/standards>

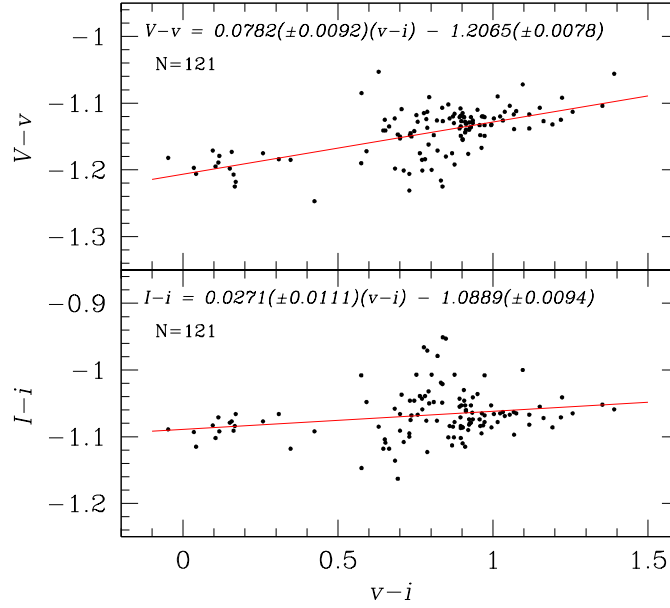


Fig. 1. Transformation relations between the instrumental and the standard photometric systems using a set of standard stars in the field of NGC 288 from the collection of Peter Stetson. *Top* and *bottom panels* correspond to the observations in the *V* and *I* filters respectively. See Section 2.2 for a discussion.

Table 2

Time-series *V* and *I* photometry for all the confirmed variables in our field of view

Variable Star ID	Filter	HJD [d]	$M_{\text{std}}$ [mag]	$m_{\text{ins}}$ [mag]	$\sigma_m$ [mag]	$f_{\text{ref}}$ [ADU/s]	$\sigma_{\text{ref}}$ [ADU/s]	$f_{\text{diff}}$ [ADU/s]	$\sigma_{\text{diff}}$ [ADU/s]	$p$
V1	V	2455542.05923	12.538	13.705	0.001	32756.433	5.278	+194.010	39.867	0.9835
V1	V	2455542.06303	12.531	13.698	0.001	32756.433	5.278	+402.337	36.651	0.9932
⋮	⋮	⋮	⋮	⋮	⋮	⋮	⋮	⋮	⋮	⋮
V2	V	2455542.05923	14.830	15.997	0.004	3897.998	5.372	+92.541	13.824	0.9835
V2	V	2455542.06303	14.836	16.004	0.004	3897.998	5.372	+69.189	13.055	0.9932
⋮	⋮	⋮	⋮	⋮	⋮	⋮	⋮	⋮	⋮	⋮
V2	I	2455542.03472	14.467	15.543	0.004	5802.472	16.287	+259.464	19.695	0.9826
V2	I	2455542.03652	14.462	15.537	0.004	5802.472	16.287	+289.454	21.511	0.9805
⋮	⋮	⋮	⋮	⋮	⋮	⋮	⋮	⋮	⋮	⋮

Standard  $M_{\text{std}}$  and instrumental  $m_{\text{ins}}$  magnitudes are listed in columns 4 and 5, respectively, corresponding to the variable star in column 1. Filter and epoch of mid-exposure are listed in columns 2 and 3, respectively. The uncertainty on  $m_{\text{ins}}$  is listed in column 6, which also corresponds to the uncertainty on  $M_{\text{std}}$ . For completeness, we also list the quantities  $f_{\text{ref}}$ ,  $f_{\text{diff}}$  and  $p$  from Eq.(1) in columns 7, 9 and 11, along with the uncertainties  $\sigma_{\text{ref}}$  and  $\sigma_{\text{diff}}$  in columns 8 and 10. This is an extract from the full table, which is available from the *Acta Astronomica Archive*.

The standard minus the instrumental magnitudes indeed show a mild dependence on the color, as can be seen in Fig. 1. We have transformed the instrumental  $v$  and  $i$  into the standard  $V$  and  $I$  magnitudes using the following equations:

$$V = v + 0.0782(\pm 0.0092)(v - i) - 1.2065(\pm 0.0078), \quad (3)$$

$$I = i + 0.0271(\pm 0.0111)(v - i) - 1.0889(\pm 0.0094). \quad (4)$$

Due to the lack of observations in the  $I$ -band for some bright saturated stars, to calculate their standard  $V$  magnitudes, we have adopted for them  $(v - i) = 0.5$  mag, which corresponds approximately to the center of the RR Lyr horizontal branch (HB).

Fig. 2 shows the RMS magnitude deviation in our  $V$  and  $I$  light curves as a function of the mean magnitude. We achieve an RMS scatter of  $\approx 10$ – $20$  mmag in both the  $V$  and  $I$  filters for stars brighter than 17 mag.

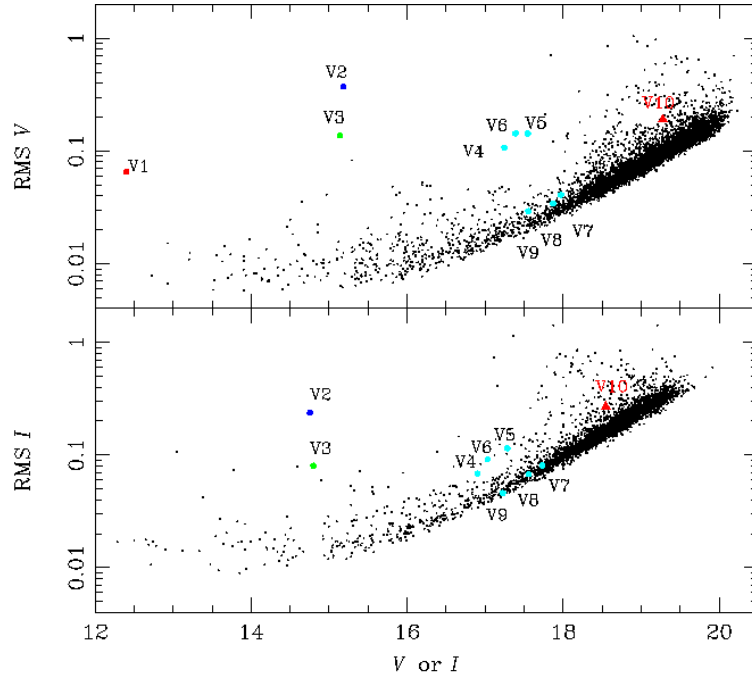


Fig. 2. The RMS magnitude deviations as a function of magnitude. The *upper and lower panels* correspond to the  $V$  and  $I$  light curves respectively. The color coding is as follows: RRab star – blue circle (V2), RRc star – green circle (V3), cyan circles are SX Phe stars (V4–V9) and red triangle is an eclipsing binary (V10). The long period variable V1 is not included in the *bottom panel* because it is saturated in the  $I$  images in our collection.

All of our  $V$  and  $I$  photometry for the variable stars in the FoV of our images of NGC 288 is reported in Table 2. Only a small portion of Table 2 is given in the printed version of this paper, while the full table is available in the electronic form from the *Acta Astronomica Archive*.

### 2.3. Astrometry

A linear astrometric solution was derived for the  $V$  filter reference image by matching  $\approx 250$  hand-picked stars with the UCAC3 star catalogue (Zacharias *et al.* 2010) using a field overlay in the image display tool GAIA (Draper 2000). We achieved a radial RMS scatter in the residuals of  $\approx 0''.3$ . The astrometric fit was then used to calculate the J2000.0 celestial coordinates for all of the confirmed variables in our field of view (see Table 3). The coordinates correspond to the epoch of the  $V$  reference image, which pertains to the heliocentric Julian day 2455542.07 d.

## 3. Search for New Variable Stars

In this section we describe the use of our time-series  $V$  and  $I$  photometry to search for new variables and to revisit the identifications, periodicities, and light curves of the known variables.

### 3.1. Search Methods

Ten variable stars listed in Table 3 all previously known, are identified in the finding chart of Fig. 6. Their distribution is apparently peculiar since they seem concentrated in a rather small off-centered region in the FoV. Before we comment on the statistical significance of this distribution we have conducted a search for new variables using our light curves. For this purpose we have used several methods which have been successful in previous studies in identifying and classifying variable stars in globular clusters. Since these methods have already been described in detail in earlier papers (*e.g.*, Arellano Ferro *et al.* 2013, Figuera Jaimes *et al.* 2013), here we only summarize them briefly.

Table 3

General data for all of the confirmed variables in NGC 288 in the FoV of our images

Variable Star ID	Variable Type	$\langle V \rangle$ [mag]	$\langle I \rangle$ [mag]	$A_V$ [mag]	$A_I$ [mag]	$P_1$ [d]	HJD <sub>max</sub> (+2450 000)	$P_2$ [d]	RA (J2000.0)	Dec. (J2000.0)
V1	SR	12.40	–	0.22	–	–	5779.2366	103. <sup>a</sup>	00 <sup>h</sup> 52 <sup>m</sup> 41 <sup>s</sup> .13	–26°33′27″.0
V2	RRab	15.237	14.788	1.137	0.74	0.6777478	5842.2373	0.67775	00 <sup>h</sup> 52 <sup>m</sup> 46 <sup>s</sup> .69	–26°34′08″.1
V3	RRc	15.177	14.829	0.387	0.24	0.4301268	5871.1484	0.4302	00 <sup>h</sup> 52 <sup>m</sup> 40 <sup>s</sup> .27	–26°32′29″.3
V4	SX Phe	17.264	16.898	0.316	0.20	0.07907489	5842.3110	0.07907	00 <sup>h</sup> 52 <sup>m</sup> 42 <sup>s</sup> .85	–26°34′46″.1
V5	SX Phe	17.589	17.284	0.414	0.34	0.05106684	5868.2112	0.05107	00 <sup>h</sup> 52 <sup>m</sup> 45 <sup>s</sup> .03	–26°33′52″.7
V6	SX Phe	17.400	17.028	0.462	0.30	0.06722082	5543.0555	0.06722	00 <sup>h</sup> 52 <sup>m</sup> 42 <sup>s</sup> .45	–26°34′55″.2
V7	SX Phe	17.981	17.730	0.077	–	0.03997368	5871.1232	0.03996	00 <sup>h</sup> 52 <sup>m</sup> 41 <sup>s</sup> .44	–26°34′00″.3
V8	SX Phe	17.875	17.555	0.061	–	0.04652840	5871.2625	0.04653	00 <sup>h</sup> 52 <sup>m</sup> 44 <sup>s</sup> .32	–26°34′00″.3
V9	SX Phe	17.558	17.223	0.04	–	0.03936761	5842.2475	0.03937	00 <sup>h</sup> 52 <sup>m</sup> 42 <sup>s</sup> .94	–26°34′10″.3
V10	E	19.275	18.545	$\approx 0.5$	$\approx 0.7$	0.4387538	5542.0865 <sup>b</sup>	0.43875	00 <sup>h</sup> 52 <sup>m</sup> 47 <sup>s</sup> .91	–26°33′02″.5

The best previous period estimates for each variable from Kaluzny *et al.* (1997) are reported in column 9 ( $P_2$ ) for comparison with our refined periods in column 7 ( $P_1$ ). The period uncertainties are within the last significant digit.

<sup>a</sup> from Oosterhoff (1943), <sup>b</sup> Time of minimum light.

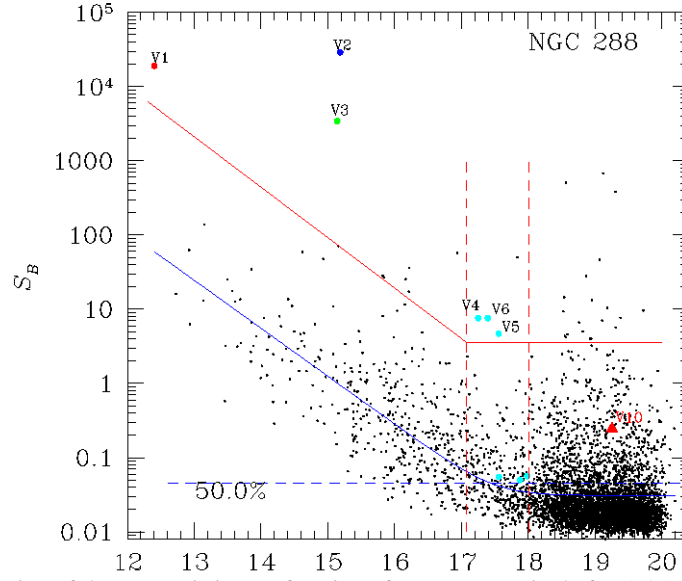


Fig. 3. Distribution of the  $S_B$  statistic as a function of mean V magnitude for 5525 stars measured in the V images of NGC 288. The colored symbols for variable stars are as described in the caption of Fig. 2. The blue lines represent the median (50%) percentile for the simulated light curves and the real distribution of  $S_B$ . The red solid line is the threshold set by eye above which one expects to find true variable stars. See the discussion in Section 3.1. The two vertical dashed red lines correspond to the magnitude limits set for the Blue Straggler region in the CMD.

Firstly, we have defined a variability statistic  $S_B$  as:

$$S_B = \frac{1}{NM} \sum_{i=1}^M \left( \frac{r_{i,1}}{\sigma_{i,1}} + \frac{r_{i,2}}{\sigma_{i,2}} + \dots + \frac{r_{i,k_i}}{\sigma_{i,k_i}} \right)^2 \quad (5)$$

where  $N$  is the total number of data points in the light curve and  $M$  is the number of groups of time-consecutive residuals of the same sign from the inverse-variance weighted mean magnitude. The residuals  $r_{i,1}$  to  $r_{i,k_i}$  form the  $i$ th group of  $k_i$  time-consecutive residuals of the same sign with corresponding uncertainties  $\sigma_{i,1}$  to  $\sigma_{i,k_i}$ . Fig. 3 shows the distribution of the  $S_B$  statistic as a function of mean magnitude for the 5525 light curves for the stars in the V images.

As in the paper by Figuera Jaimes *et al.* (2013) we calculated  $10^6$  randomly generated light curves (their Eq. 4) and computed their  $S_B$  values. The median of the distribution, or 50% percentile is indicated by the dashed blue line in Fig. 3. The fit to the real  $S_B$  values is shown as a solid blue line for  $V > 18$  mag and we notice that the real and the simulated values are very close, *i.e.*, the simulations are a good description of the statistical noise for these faint stars. For brighter stars however ( $V < 18$  mag) systematic errors dominate and  $S_B$  increases logarithmically with stellar magnitude. As before, the solid blue line is the fit to the real distribution of  $S_B$ . Then, guided by the distribution of the known variables, we defined by eye a variability detection threshold indicated by the solid red line in Fig. 3. RR Lyr stars are generally easily identified by this method as they have substantially larger



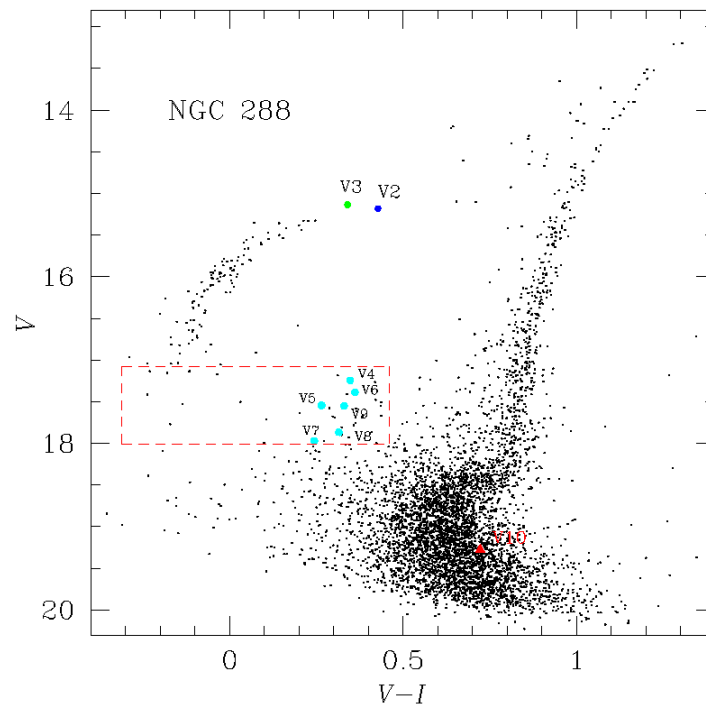


Fig. 4. Color-magnitude diagram of NGC 288. The colored symbols are as in the caption of Fig. 2. The long period variable V1 is not included because it is saturated in the  $I$  images in our collection.

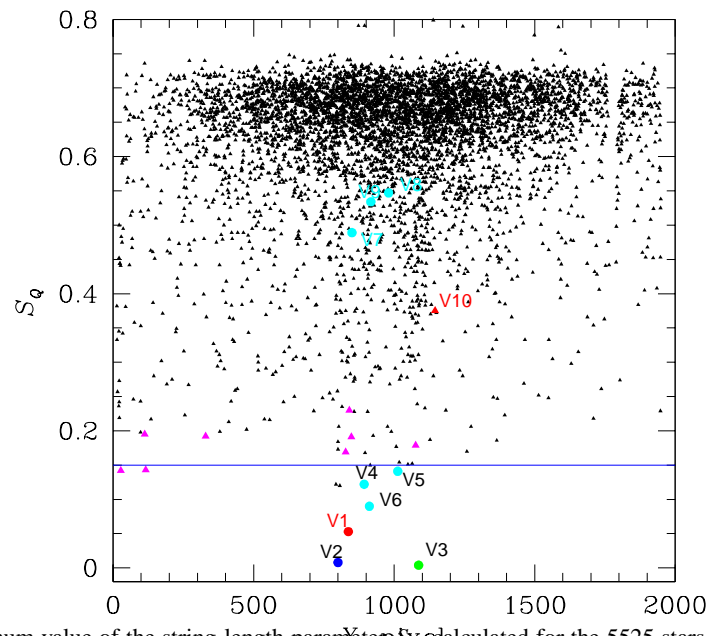


Fig. 5. Minimum value of the string-length parameter  $S_q$  calculated for the 5525 stars with  $V$  light curves vs. the CCD  $x$ -coordinate. The colored symbols are as described in the caption of Fig. 2.

values of  $S_B$  among stars of their magnitude range. The same is true of the SR long-term variables. Short-period small-amplitude SX Phe stars might however escape detection by this approach. As it can be seen in Fig. 3 the three large amplitude SX Phe stars (V4, V5 and V6) are found clearly above the threshold. However the three low amplitude ones (V7, V8, and V9) and the known binary star (V10) are buried below in the cloud of otherwise non-variable stars.

Only seven stars brighter than 17 mag and one in the BS region (between the two dashed red lines) have  $S_B$  larger than the detection threshold. We have explored their  $V$  and  $I$  light curves in detail. No convincing signs of true variability were found. For several of them their large  $S_B$  is explained by their proximity to an authentic known variable star or to a poorly subtracted bright star, hence their difference fluxes suffer correlated systematic errors.

A second strategy that we applied was the string-length method (Burke, Rolland and Boy 1970, Dworetsky 1983) to each light curve to determine the period and a normalized string-length statistic  $S_Q$ . In Fig. 5 we plot the minimum  $S_Q$  value for each light curve as a function of their corresponding CCD  $x$ -coordinate. The known variables are plotted with the colored symbols as described in the caption. The horizontal blue line is not a statistically defined threshold but again, set by eye, as an upper limit to the majority of the known variables. In fact this method could recover variables V1 to V6 but also fails in detecting the low-amplitude short-period variables V7 to V10. The eight stars spotted before as having large  $S_B$  values are plotted with purple triangles and we note that only two would pass the  $S_Q$  threshold requirement. There are six other stars below the  $S_Q$  threshold line. However, as before, the exploration of their light curves did not reveal any true variability.

Finally, we have followed a third approach to identify variables in the field of our images by detecting PSF-like peaks in a stacked image built from the sum of the absolute valued difference images normalized by the standard deviation in each pixel as described by Bramich *et al.* (2011). This method allowed us to confirm the variability of all ten known variables in Table 3 but no new variables emerged.

In conclusion, we did not find any new variable stars in our light curve collection using the above three methods. We believe that our search for variable stars with continuous variations (*i.e.*, not eclipsing binaries) is fairly complete down to  $V \approx 18$  mag for amplitudes larger than  $\approx 0.05$  mag and periods between  $\approx 0.02$  d and a few hundred days.

### 3.2. Period Determination and Refinement

We have combined our  $V$  light curves with those of Kaluzny *et al.* (1997), taken between 1990 and 1992, and of Kaluzny (1996), taken in 1995, to re-calculate the periods. Since more than twenty years have passed between the two data sets, their combination leads to substantially refined periods.

We have noticed small zero point differences of 0.02 mag to 0.08 mag between

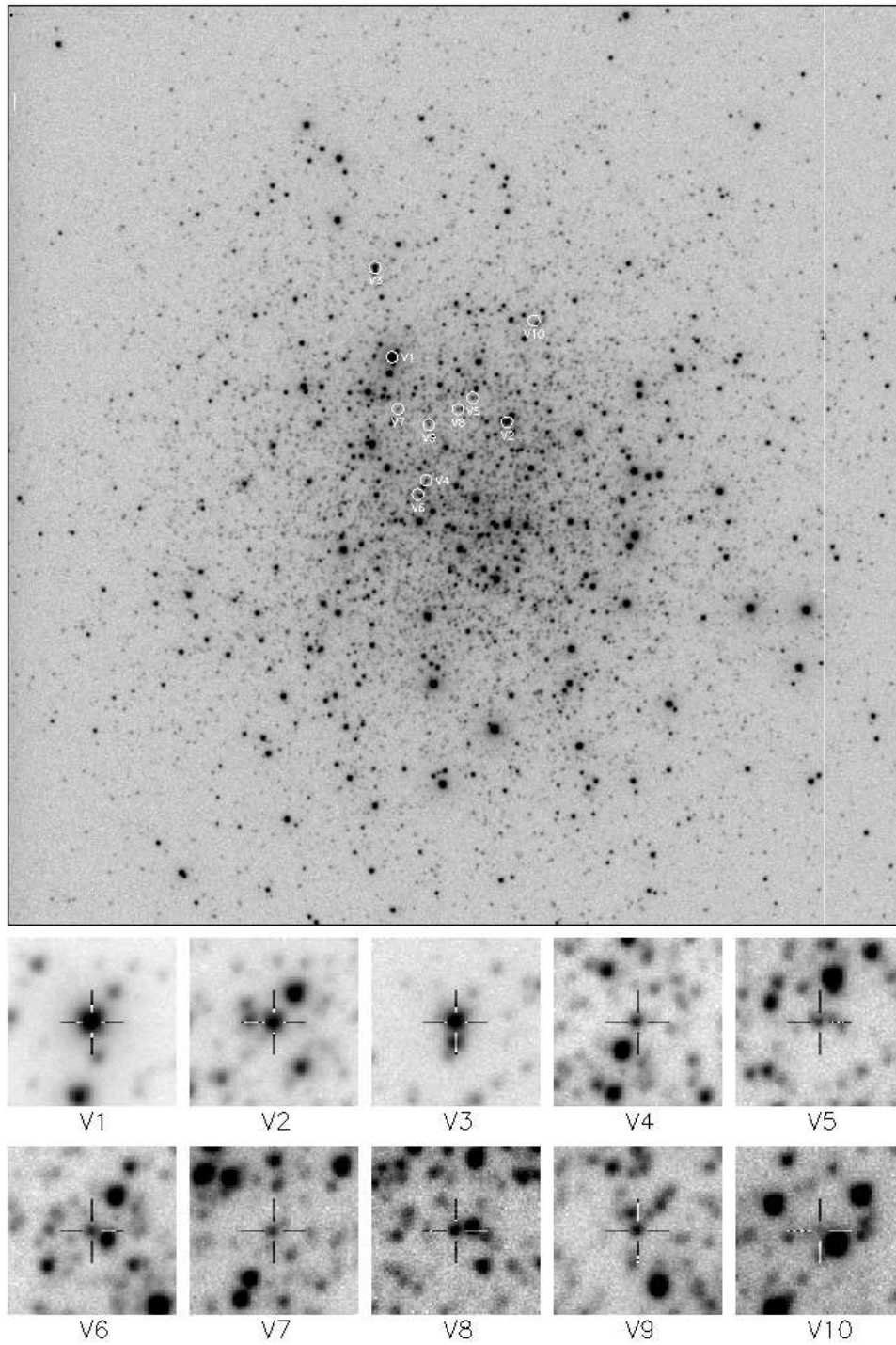


Fig. 6. Finding charts constructed from our Hanle V reference image. North is up and East is to the right. The cluster image is  $9.62 \times 9.87 \text{ arcmin}^2$ , and the image stamps are of size  $23.7 \times 23.7 \text{ arcsec}^2$ . Each variable lies at the center of its corresponding image stamp and is marked by a cross-hair.

our light curves and those of Kaluzny *et al.* (1997). This is to be expected since the error in the reference flux affects all photometric measurements for a single star in the same way. The procedure to estimate the refined period was as follows: first we estimated the period using the combined data sets and the program period04 (Lenz and Breger 2005) and used this to phase the light curves. The necessary magnitude shift was applied to the data from Kaluzny (1996) and Kaluzny *et al.* (1997) and then the leveled combined light curve was period analyzed using a dense scan of the string-length method within a short period range around the initial estimate of the period. The new periods are given in column 7 of Table 3 and have been used to phase the light curves shown in Figs. 7 and 9. Variations of the period within the last significant digit can spoil the phasing of the light curve, which sets the uncertainty of the periods. As a reference we list the periods from Kaluzny *et al.* (1997) in column 9.

#### 4. RR Lyrae Stars

##### 4.1. Physical Parameters from Light Curve Fourier Decomposition

An estimation of  $[\text{Fe}/\text{H}]$ ,  $M_V$ , and  $T_{\text{eff}}$  for a given RR Lyr star can be obtained by Fourier decomposing the light curve into its harmonics as

$$m(t) = A_0 + \sum_{k=1}^N A_k \cos\left(\frac{2\pi}{P}k(t - E) + \phi_k\right) \quad (6)$$

where  $m(t)$  are magnitudes at time  $t$ ,  $P$  the period and  $E$  the epoch. A linear minimization routine is used to fit the data with the Fourier series model, deriving the best fit values of the amplitudes  $A_k$  and phases  $\phi_k$  of the sinusoidal components. From the amplitudes and phases of the harmonics in Eq.(6) the Fourier parameters  $\phi_{ij} = j\phi_i - i\phi_j$  and  $R_{ij} = A_i/A_j$  are computed.

These Fourier parameters can be used in the semi-empirical calibrations of Jurcsik and Kovács (1996), for RRab stars, and Morgan, Wahl and Wieckhorts (2007), for RRC stars, to obtain  $[\text{Fe}/\text{H}]_{\text{ZW}}$  on the Zinn and West (1984) scale. The absolute magnitude  $M_V$  can be estimated from the calibrations of Kovács and Walker (2001) for RRab stars and of Kovács (1998) for the RRC stars. The effective temperature  $T_{\text{eff}}$  was estimated using the calibration of Jurcsik (1998). For brevity we do not present here the specific equations but they can be found in a recent paper (Arellano Ferro *et al.* 2013).

The mean magnitudes  $A_0$ , and the Fourier light curve fitting parameters for V2 (RRab) and V3 (RRC) in the  $V$  filter are listed in Table 4. The absolute magnitude  $M_V$  was converted into  $\log L/L_{\odot} = -0.4(M_V - M_{\text{bol}} + BC)$ . The bolometric correction was calculated using the formula  $BC = 0.06[\text{Fe}/\text{H}]_{\text{ZW}} + 0.06$  given by Sandage and Cacciari (1990). We adopted the value  $M_{\text{bol}}^{\odot} = 4.75$  mag.

The resulting physical parameters are given in Table 5. The average metallicity obtained from the RRab and RRC stars is  $[\text{Fe}/\text{H}]_{\text{ZW}} = -1.62 \pm 0.02$  which can be

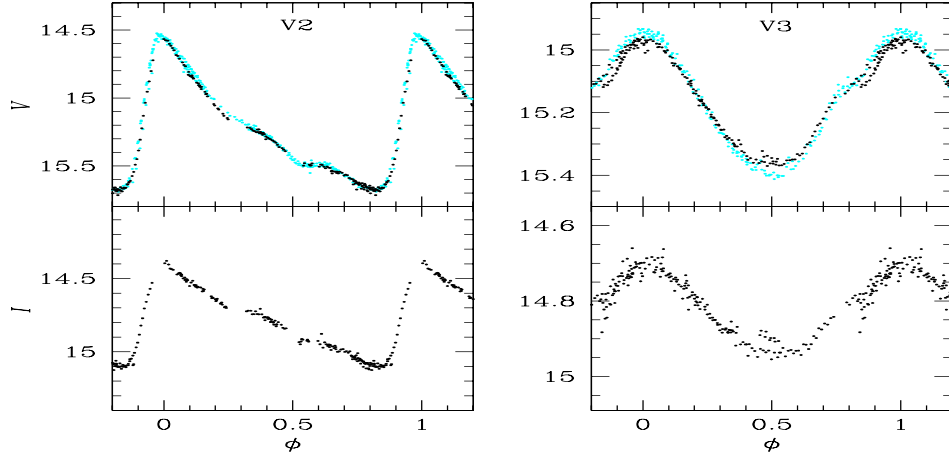


Fig. 7. Standard magnitude  $V$  and  $I$  light curves of the RR Lyr stars V2 and V3 phased with the periods listed in Table 3. Black points represent Hanle data from the present work. Blue points represent  $V$  data from Kaluzny *et al.* (1997). Typical uncertainties in  $V$  and  $I$  are  $\approx 6$  mmag.

Table 4

Fourier coefficients  $A_k$  for  $k = 0, 1, 2, 3, 4$ , and phases  $\phi_{21}$ ,  $\phi_{31}$  and  $\phi_{41}$ , for V2 (RRab) and V3 (RRc) in NGC 288

Variable ID	$A_0$ [V mag]	$A_1$ [V mag]	$A_2$ [V mag]	$A_3$ [V mag]	$A_4$ [V mag]	$\phi_{21}$	$\phi_{31}$	$\phi_{41}$	$N$	$D_m$
V2	15.237(1)	0.401(2)	0.204(2)	0.138(2)	0.065(2)	4.257(12)	8.513(18)	6.805(34)	9	3.5
V3	15.177(1)	0.188(2)	0.008(1)	0.014(1)	0.011(1)	2.023(170)	5.115(99)	3.396(130)	6	–

The numbers in parentheses indicate the uncertainty on the last decimal place. Also listed are the number of harmonics  $N$  used to fit the light curve of each variable and the deviation parameter  $D_m$  (see Section 4.1).

converted to the new scale defined by Carretta *et al.* (2009) using UVES spectra of RGB stars in globular clusters by

$$[\text{Fe}/\text{H}]_{\text{UVES}} = -0.413 + 0.130[\text{Fe}/\text{H}]_{\text{ZW}} - 0.356[\text{Fe}/\text{H}]_{\text{ZW}}^2. \quad (7)$$

We find  $[\text{Fe}/\text{H}]_{\text{UVES}} = -1.56 \pm 0.03$ . No previous estimates of  $[\text{Fe}/\text{H}]$  from Fourier decomposition of the RR Lyr light curves exist for this cluster.

Zinn (1980) made an early estimation of iron content of NGC 288 from integrated photometry in the  $Q_{39}$  index. He found  $[\text{Fe}/\text{H}] = -1.61$ . Zinn and West (1984) summarized previous estimates of  $[\text{Fe}/\text{H}]$  given in earlier papers in a variety of metallicity scales (their Table 5). They report the weighted average  $[\text{Fe}/\text{H}]_{\text{ZW}} = -1.40$  in their new scale. The high resolution spectroscopic value of  $[\text{Fe}/\text{H}]$ , derived by Carretta and Bragaglia (1998) from two giant cluster member stars is  $-1.07$  in their own scale which is equivalent to  $[\text{Fe}/\text{H}]_{\text{ZW}} = -1.40$

Table 5  
Physical parameters for V2 (RRab) and V3 (RRc) stars

Star	$[\text{Fe}/\text{H}]_{\text{ZW}}$	$M_V$	$\log(L/L_\odot)$	$\log T_{\text{eff}}$	$M/M_\odot$	$R/R_\odot$
V2	-1.642(17)	0.376(3)	1.750(1)	3.800(8)	0.74(7)	6.04(1)
V3	-1.59(24)	0.579(7)	1.668(1) <sup>a</sup>	3.856(1)	0.38(1) <sup>a</sup>	5.57(9)

<sup>a</sup>These values depend on  $M_V$  whose peculiarity for V3 is discussed in Section 4.2. The numbers in parentheses indicate the uncertainty on the last decimal place and have been calculated as described in the text.

in the Zinn and West (1984) scale. Our calculation from two independent calibrations for RRab and RRc stars of the Fourier decomposition parameters average  $[\text{Fe}/\text{H}]_{\text{ZW}} = -1.62 \pm 0.02$  (statistical)  $\pm 0.14$  (systematic), favors a lower iron content.

#### 4.2. Distance to NGC 288 from the RR Lyr Stars

The  $M_V$  value calculated for the RRab and RRc stars in Table 5 can be used to estimate the true distance modulus. Given the fact that these  $M_V$  values come from independent calibrations for the RRab and RRc stars, with their own systematic uncertainties, we should consider the distances as derived from them as two independent estimations. We adopted  $E(B - V) = 0.03$  mag (Buonanno *et al.* 1984, Harris 1996). We find the true distance moduli of  $14.768 \pm 0.003$  mag and  $14.505 \pm 0.008$  mag using the RRab and RRc stars respectively. The uncertainties are only the internal errors which are small. These moduli correspond to the distances 8.99 kpc and 7.96 kpc with corresponding internal and systematic errors of  $\approx 0.01$  kpc and  $\approx 0.17$  kpc respectively. The distance to NGC 288 listed in the catalogue of Harris (1996, 2010 edition) is 8.9 kpc.

The distance obtained from the RRc star, V3, is discrepant when compared with that from the RRab star and the generally accepted distance for the cluster. In Fig. 8 we plot  $\phi_{21}^{(s)}$  vs.  $P$ , which are the key parameters for the calculation of  $M_V$  in RRc stars (see Eq. 13 of Arellano Ferro *et al.* 2013), for a group of RRc stars in several globular clusters listed in the caption of Fig. 8. The corresponding data have been taken from recent publications of our working group on those clusters. V3 is a long period RRc star and its  $\phi_{21}^{(s)}$  value is very small, these two facts highlight the star as peculiar. The other stars that stand out from the distribution of RRc stars are the long period V13 in NGC 4147 and the short period variable V92 in M53. V13 was found by Arellano Ferro *et al.* (2004), to exhibit amplitude variations, probably due to the Blazhko effect, while V92 shows an unusual low amplitude (Arellano Ferro *et al.* 2011). We have noticed in Fig. 7 the amplitude difference in the light curves of V3 from Kaluzny *et al.* (1997) data and that from the present

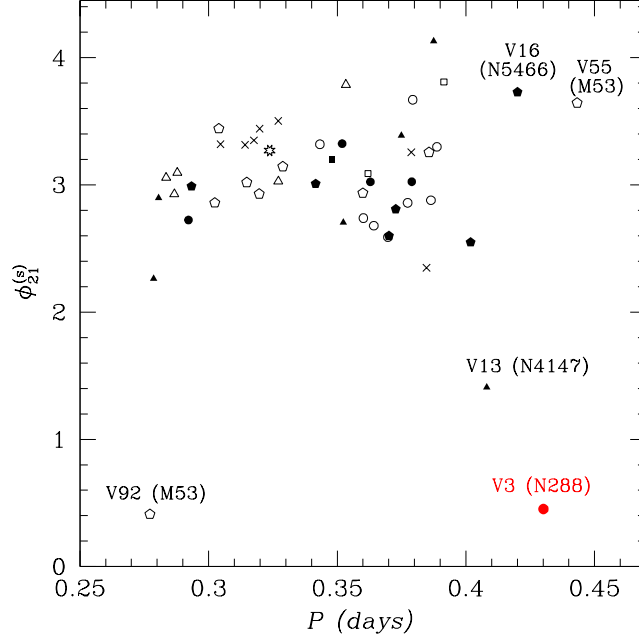


Fig. 8. Distribution of RRc stars from a family of clusters in the  $\phi_{21}^{(s)}-P$  plane. Symbol codes and data sources are: filled triangles NGC 4147 (Arellano Ferro *et al.* 2004), open circles M15 (Arellano Ferro, García Lugo and Rosenzweig 2006), M2 open squares (Lázaro *et al.* 2006), NGC 5466 filled pentagons (Arellano Ferro *et al.* 2008), NGC 5053 filled circles (Arellano Ferro, Giridhar and Bramich 2010), M72 open triangles (Bramich *et al.* 2011), M53 open pentagons (Arellano Ferro *et al.* 2011), M79 starred circle (Kains *et al.* 2012), M30 filled square (Kains *et al.* 2013), M9 crosses (Arellano Ferro *et al.* 2013). In the long period range V3 in NGC 288 and V13 in NGC 4147 stand out from the distribution. The short period star V92 in M53 is also peculiar. See text in Section 4.2 for a discussion.

work. While we remark that this amplitude difference may be an artefact from the reduction processes of both data sets, or that the presence of the Blazhko effect cannot be ruled out, with the present data we cannot identify the reason for the peculiar position of V3 in the  $\phi_{21}^{(s)}-P$  plane. Due to these peculiarities, we do not give any weight to the distance suggested by V3.

#### 4.3. RR Lyr Masses and Radii

Given the period, luminosity and temperature for each RR Lyr star, its mass and radius can be estimated from the equations:  $\log M/M_{\odot} = 16.907 - 1.47 \log P_F + 1.24 \log(L/L_{\odot}) - 5.12 \log T_{\text{eff}}$  (van Albada and Baker 1971) and  $L = 4\pi R^2 \sigma T^4$  respectively. The masses and radii are given in Table 5 in solar units. Given the peculiarity of  $M_V$  for V3 (see Section 4.2),  $\log(L/L_{\odot})$  and  $\log M/M_{\odot}$  should be considered with caution for this star.

### 5. SX Phoenicis Stars

Six SX Phe stars are known in NGC 288, three of large amplitude (V4, V5 and V6) and three of low amplitude (V7, V8, V9). We have searched the light curves of all stars in an arbitrarily defined blue straggler region in the CMD of Fig. 4 delimited by the dashed red lines. As discussed in Section 3.1 all our approaches to finding variable stars failed to reveal any convincing new variables.

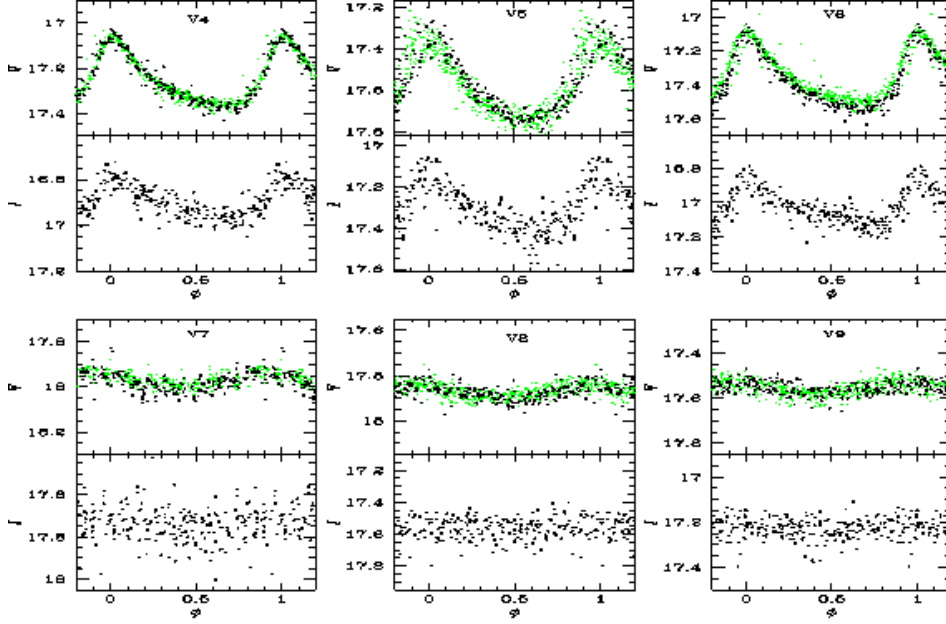


Fig. 9. Light curves of the SX Phe stars. Green symbols are from Kaluzny (1996) and Kaluzny *et al.* (1997) and black symbols from the present work. Typical uncertainties are 0.03 mag and 0.05 mag for V and I respectively.

The light curves of the six known SX Phe are shown in Fig. 9 phased with the refined periods and epochs listed in Table 3. We have included the data from Kaluzny (1996) and Kaluzny *et al.* (1997) (green symbols). Our I light curves are also shown in the bottom panels.

It is worth noting that V5 has a larger dispersion than V4 and V6 despite being of similar magnitudes. We searched for a secondary frequency by prewhitening the primary frequency  $f_1 = 19.5821790 \pm 0.0000016 \text{ d}^{-1}$  and its aliases. In Fig. 10 we note the presence of a secondary frequency at  $f_2 = 25.1482392 \pm 0.0000054 \text{ d}^{-1}$ . The ratio  $f_1/f_2 = 0.779$  lead us to identify  $f_1$  and  $f_2$  with the fundamental and the first overtone radial modes respectively.

Fig. 11 shows P–L diagram for the SX Phe stars. Except for V9, the known SX Phe define a linear progression similar to the SX Phe in other globular clusters (*e.g.*, M53 Arellano Ferro *et al.* 2011 and Jeon *et al.* 2003, and M55 Pych *et al.* 2001). We adopted the SX Phe P–L relation derived by Arellano Ferro *et al.* (2011)



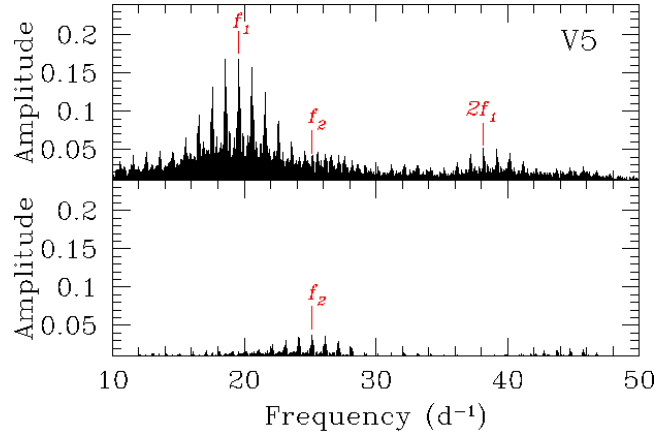


Fig. 10. Frequency spectra of V5 calculated from the  $V$  light curve of Fig. 9. The primary frequency  $f_1$ , its alias at  $2f_1$  and secondary frequency  $f_2$  are labelled. Since  $f_1/f_2 = 0.779$  we interpret this as being a double mode pulsator with the fundamental and the first overtones being excited.

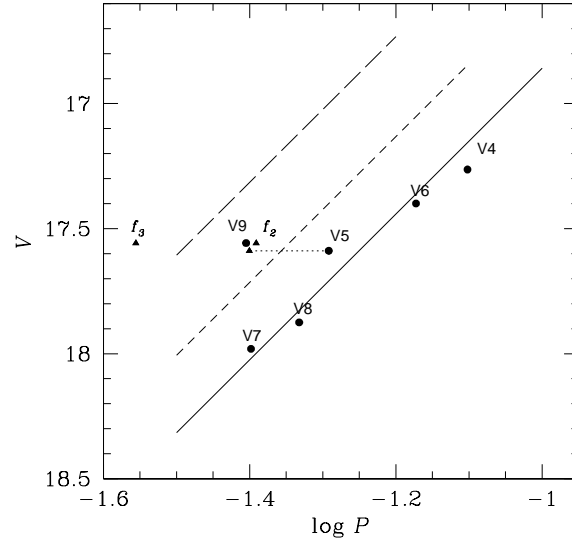


Fig. 11. P-L relation for SX Phe stars. The solid line corresponds to the SX Phe P-L relation of Arellano Ferro *et al.* (2011) derived in M53 scaled to a distance of 8.9 kpc. Short and long dashed lines represent the loci of the corresponding first and second overtone respectively. For V5 we represent the fundamental mode (filled circle) and the first overtone (black triangle) modes joined by the dotted line. For V9 we indicate the positions of secondary frequencies  $f_2$  and  $f_3$  which are interpreted as a non-radial mode and the second overtone, respectively.

in M53,  $M_V = -2.916 \log P - 0.898$ , to calculate  $M_V$  and hence the distance for each SX Phe star. The average distance (excluding V9) is  $8.9 \pm 0.3$  kpc. The solid line in Fig. 11 is the  $V - \log P$  relation corresponding to a distance of 8.9 kpc. As it is seen the match with the SX Phe distribution is very good. V5 lies slightly above the relation but we have noted that it is blended with a fainter star. There is a clear indication that V9 is pulsating in an overtone mode.

The above independent estimation of the distance is in excellent agreement with the distance derived from the Fourier decomposition of the RRab star V2 and with the generally adopted distance (8.9 kpc Harris 1996).

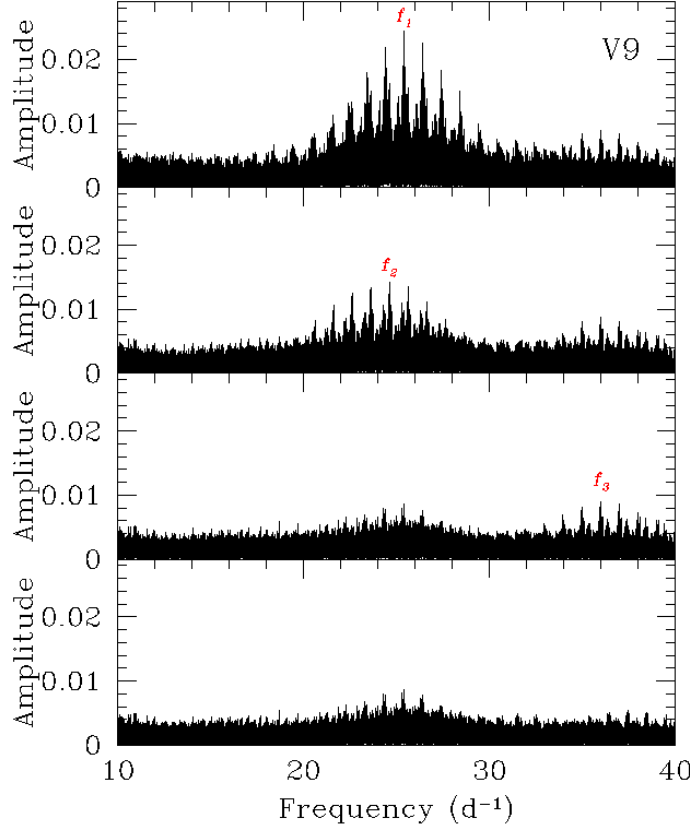


Fig. 12. Frequency spectra of V9 calculated from the *V* light curve of Fig. 9. The secondary frequencies  $f_2$  and  $f_3$  are labelled and discussed in Section 5.

Then the question arises: if all known SX Phe stars in NGC 288 pulsate in the fundamental mode (except V9), why do some have a very large amplitude (V4, V5, V6) and some a very small one (V7 and V8)? We explore the possibility of more than one mode being excited in the small amplitude stars. Using the frequency finding program *period04* (Lenz and Breger 2005) we have prewhitened the main frequency, and in all cases except V9 we found no signs of secondary frequencies. Therefore, V9 deserves special attention. In Fig. 12 the frequency spectra calculated on the *V* light curves are shown. The top panel corresponds to the original data, where the main frequency  $f_1 = 25.4015993 \text{ d}^{-1}$  agrees well with the period found from the string-length method (Table 3). The middle panel corresponds to the spectrum after prewhitening the main frequency. The residuals show a frequency of  $f_2 = 24.61423 \text{ d}^{-1}$ . As the residual signal is substantial a second prewhitening was performed to find a frequency of  $f_3 = 35.95981 \text{ d}^{-1}$ . The ratio  $f_1/f_3=0.706$

is a bit off the canonical value 0.783 for the fundamental and first overtone modes (Santolamazza *et al.* 2001, Poretti *et al.* 2005). After removing  $f_3$  the signal virtually disappears; however some signal remains around  $f_1$ , which probably indicates that we have not fully succeeded in determining and removing the primary frequency, which given the scatter in the light curve is probably not surprising. On the other hand our frequency ratio of 0.706 is very close to the ratio between first and second overtone which is 0.729. In Fig. 11 we have also included the positions of V9 corresponding to the frequencies  $f_2$  and  $f_3$  (black triangles). If one identifies  $f_1$  and  $f_3$  with the first and second overtone frequencies respectively, this strongly suggests that V9 is a double-mode SX Phe pulsating simultaneously in the first and second overtones while  $f_2$  probably corresponds to a non-radial mode.

However, it is clear that this is a multifrequency variable, which accounts for its very small amplitude. The fact that we did not find secondary frequencies in the spectra of the other two small amplitude SX Phe stars, V7 and V8, is intriguing.

## 6. On the Variability of V1 and V10

These two stars are a bright long period variable and a faint contact binary respectively. Here we offer some comments on their variability and periods.

*V1.* The variability of this star was discovered by Oosterhoff (1943) on photographic plates taken between 1928 and 1930. Despite the time elapsed, the phase coverage in Oosterhoff's light curve continues to be the best available. In Fig. 13 we plot the light curves from 1928–1930 and 2010–2013. A period analysis exclusively using the old data gives a period of 103 d, as reported by Oosterhoff. Unfortunately it is not very clear how Oosterhoff calculated the mean brightness reported in his Table 1, thus despite the fact that we have  $V$  magnitudes for V1 and one of the comparison stars used by Oosterhoff (star  $b$  in his chart), we refrain from attempting to bring the old measurements into a similar magnitude scale.

*V10.* This is a very faint eclipsing binary discovered by Kaluzny *et al.* (1997). Its membership in NGC 288 was addressed by Rucinski (2000) who considers it a cluster member after comparing its value of  $M_V$  derived for the cluster distance modulus and the one implied by a  $M_V - \log P - (B - V)$  relationship.

In Fig. 14 the light curves in our  $V$  and  $I$  data are shown along with  $V$  data from Kaluzny *et al.* (1997) phased with the refined period given in Table 3.

## 7. Summary and Conclusions

A deep search for variability in the RGB, HB, BS and turnoff point (down to  $V \approx 19$  mag) regions of the globular cluster NGC 288 was conducted but new variables were not found. Thus, we can claim that in the FoV of our images the census of cluster RR Lyr stars is complete (except where the bad pixel column lies, see finding chart in Fig. 6) and that if unknown SX Phe stars do exist in the cluster

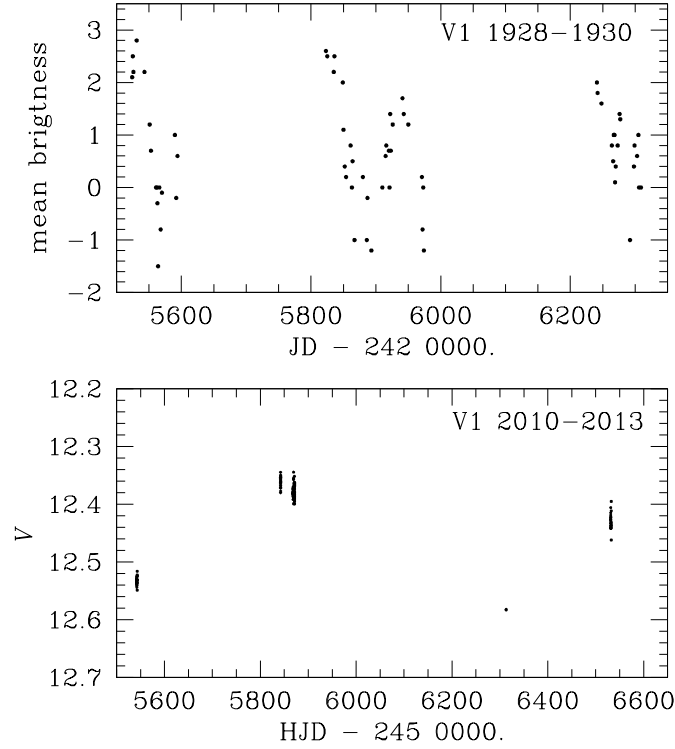


Fig. 13. Light curves of the SR star V1. *Top panel:* the differential mean brightness from Table 1 of the discovery paper (Oosterhoff 1943). A period analysis of these data confirms the 103d period reported by Oosterhoff. *Bottom panel:* the variations from our  $V$  photometry.

they must be of amplitudes smaller than the detection limit of our data.

We addressed the apparent off-center distribution of the variables stars. We investigated the distribution of the SX Phe stars in this cluster by comparing it to the spatial distribution of all blue straggler stars (BSS). This is similar to what was done by Kains *et al.* (2012) for the peculiar distribution of RR Lyr stars in NGC 1904 (M79). We first looked at the angular distribution of the six SX Phe stars in our sample, *i.e.*, how “close together” our SX Phe stars are, and compared it to randomly drawn samples of six BSS. We find that the angular distribution of the detected SX Phe stars is smaller than 83% of the randomly drawn samples, which is not significant given the small sample size. We also looked at the centroid position of the randomly drawn samples with respect to the center of the cluster as estimated from our reference image. From this we found that although visually the stars appear off-center, the offset of their centroid with the center of the cluster is very close to the most probable value found from the random samples, with 45% of the samples having a centroid further from the center of the cluster than our SX Phe sample.

The Fourier decomposition of the light curves of one RRab and one RRC star was performed to calculate the values of  $[\text{Fe}/\text{H}]$ ,  $M_V$ ,  $\log L/L_\odot$ ,  $T_{\text{eff}}$ , the stellar

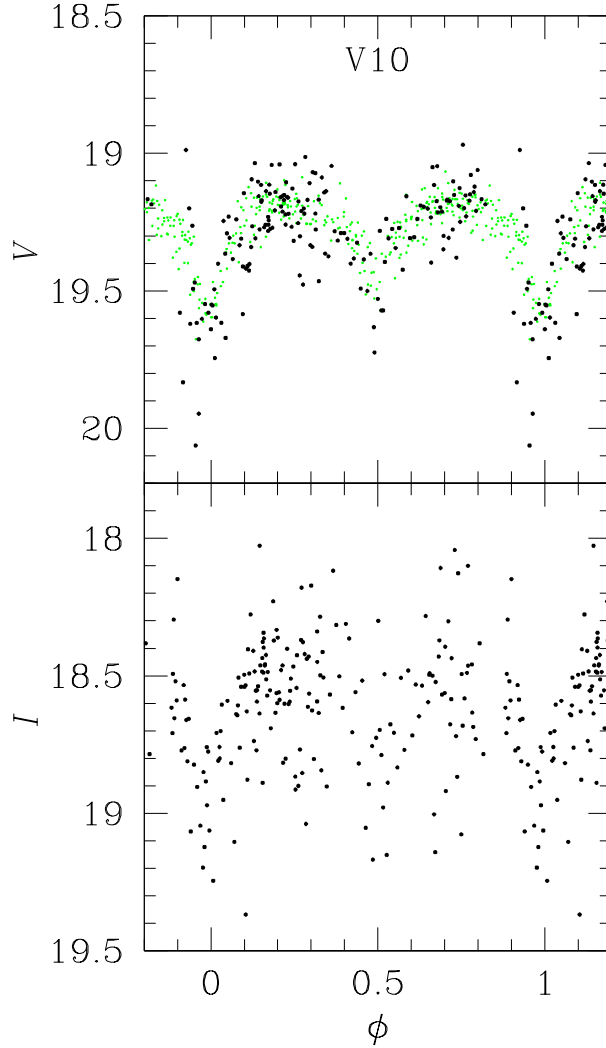


Fig. 14.  $V$  and  $I$  light curves of V10 with the data from Kaluzny (1996) and Kaluzny *et al.* (1997) (green circles) and our data (black circles). Both data sets have been used to refine the period in Table 4.

radius and mass, using *ad hoc* semi empirical calibrations (Jurcsik and Kovács 1996, Morgan *et al.* 2007, Kovács and Walker (2001) and Kovács (1998).

The mean value of the iron abundance obtained from the two RR Lyr stars in the cluster is  $[\text{Fe}/\text{H}]_{\text{ZW}} = -1.62 \pm 0.02$  (statistical)  $\pm 0.14$  (systematic) in the Zinn and West (1984) scale or  $[\text{Fe}/\text{H}]_{\text{UVES}} = -1.56 \pm 0.03$  (statistical)  $\pm 0.20$  (systematic) in the scale defined more recently by Carretta *et al.* (2009). The absolute magnitudes of the RRab and RRC stars lead to significantly different distances: from the RRab (V2) we find a distance of 8.99 kpc while from the RRC we find 7.96 kpc (with internal statistical error of  $\approx 0.003$  kpc) but we have noted that the

relevant Fourier parameter  $\phi_{21}$  is peculiar in V3. An independent estimate of the cluster distance was made from the individual stellar distances obtained from the P–L relation of the SX Phe stars (Arellano Ferro *et al.* 2011). We found an average distance of  $8.9 \pm 0.3$  kpc.

Finally, we identified the two SX Phe stars, V5 and V9, as double-mode pulsators. V5 is pulsating in the fundamental and the first overtone while V9 seems to be pulsating in the first and second overtones plus a non-radial mode.

**Acknowledgements.** We are grateful to the TAC of the IAO for generous telescope time allocation to this project and to the support astronomers of IAO, at Hanle and CREST (Hosakote) for their very efficient help while acquiring the data. AAF is grateful to ESO-Garching for warm hospitality during the production of this paper. This project was supported by DGAPA-UNAM grant through project IN104612.

We have made a large use of the SIMBAD and ADS services for this investigation.

## REFERENCES

- Arellano Ferro, A., Arévalo, M. J., Lázaro, C., Rey, M., Bramich, D.M., and Giridhar, S. 2004, *Revista Mexicana de Astronomía y Astrofísica*, **40**, 209.
- Arellano Ferro, A., García Lugo, G., and Rosenzweig, P. 2006, *Revista Mexicana de Astronomía y Astrofísica*, **42**, 75.
- Arellano Ferro, A., Rojas López, V., Giridhar, S., and Bramich, D.M. 2008, *MNRAS*, **384**, 1444.
- Arellano Ferro, A., Giridhar, S., and Bramich, D.M. 2010, *MNRAS*, **402**, 226.
- Arellano Ferro, A., Figuera Jaimes, R., Giridhar, Sunetra, Bramich, D.M., Hernández Santisteban, J.V., and Kuppuswamy, K. 2011, *MNRAS*, **416**, 2265.
- Arellano Ferro, A., *et al.* 2013, *MNRAS*, **434**, 1220.
- Bramich D.M. 2008, *MNRAS*, **386**, L77.
- Bramich D.M., Figuera Jaimes R., Giridhar S., and Arellano Ferro, A. 2011, *MNRAS*, **413**, 1275.
- Bramich, D.M., and Freudling, W. 2012, *MNRAS*, **424**, 1584.
- Bramich D.M., *et al.* 2013, *MNRAS*, **428**, 2275.
- Buonanno, R., Corsi, C. E., Fusi Pecci, F., Alcaïno, G., and Liller, W. 1984, *A&AS*, **57**, 75.
- Burke E.W., Rolland W.W., and Boy W.R. 1970, *Journal of the Royal Astronomical Society of Canada*, **64**, 353.
- Carretta, E., and Bragaglia, A. 1998, *A&A*, **329**, 937.
- Carretta, E., and Bragaglia, A., Gratton, R., D’Orazi, V., and Lucatello, S. 2009, *A&A*, **508**, 695.
- Draper, P.W. 2000, *ASP Conf. Ser.*, **216**, Eds. Manset N., Veillet C., Crabtree D., p. 615.
- Dworetzky, M.M. 1983, *MNRAS*, **203**, 917.
- Figuera Jaimes, R., Arellano Ferro, A., Bramich, D.M., and Giridhar, S. 2013, *A&A*, **556**, A20.
- Harris, W.E. 1996, *AJ*, **112**, 1487.
- Hollingsworth, L.M., and Liller, M.H. 1977, *IBVS*, 1360.
- Jeon, Y.-B., Lee, M.G., Kim, S.-L., and Lee, H. 2003, *AJ*, **125**, 3165.
- Jurcsik, J. 1995, *Acta Astron.*, **45**, 653.
- Jurcsik, J. 1998, *A&A*, **333**, 571.
- Jurcsik, J., and Kovács, G. 1996, *A&A*, **312**, 111.
- Kains, N., Bramich, D.M., Figuera Jaimes, R., Arellano Ferro, A., Giridhar, S., and Kuppuswamy, K. 2012, *A&A*, **548**, A92.

- Kains, N., *et al.* 2013, *A&A*, **555**, A36.
- Kaluzny, J. 1996, *A&AS*, **120**, 83.
- Kaluzny, J., Krzeminski, W., and Nalezyty, M. 1997, *A&AS*, **125**, 337.
- Kovács, G. 1998, *Memorie della Società Astronomia Italiana*, **69**, 49.
- Kovács, G., and Walker, A.R. 2001, *A&A*, **371**, 579.
- Lázaro, C., Arellano Ferro, A., Arévalo, M.J., Bramich, D.M., Giridhar, S., and Poretti, E. 2006, *MNRAS*, **372**, 69.
- Lenz, P., and Breger M. 2005, *Communications in Asteroseismology*, **146**, 53.
- Morgan, S., Wahl, J.N., and Wieckhorts, R.M. 2007, *MNRAS*, **374**, 1421.
- Oosterhoff, P.Th. 1943, *Bulletin of the Astronomical Institutes of the Netherlands*, **9**, 397.
- Pietrukowicz, P., Kaluzny, J., Schwarzenberg-Czerny, A., Thompson, I.B., Pych, W., Krzeminski, W., and Mazur, B. 2008, *MNRAS*, **388**, 1111.
- Poretti, E., *et al.* 2005, *A&A*, **440**, 1097.
- Pych, W., Kaluzny, J., Krzeminski, W., Schwarzenberg-Czerny, A., and Thompson, I.B. 2001, *A&A*, **367**, 148.
- Rucinski, S.M. 2000, *AJ*, **120**, 319.
- Sandage, A., and Cacciari, C. 1990, *ApJ*, **350**, 645.
- Santolamazza, P., Marconi, M., Bono, G., Caputo, F., Cassisi, S., and Gilliland, R.L. 2001, *ApJ*, **554**, 1124.
- Stetson, P.B. 2000, *PASP*, **112**, 925.
- van Albada, T.S., and Baker, N. 1971, *ApJ*, **169**, 311.
- Zacharias, N., *et al.* 2010, *AJ*, **139**, 2148.
- Zinn, R. 1980, *ApJS*, **42**, 19.
- Zinn, R., and West, M. J. 1984, *ApJS*, **55**, 45.